NASA CR-66785



# DRAG COEFFICIENTS FOR SPHERES FOR FREE MOLECULAR FLOW IN $N_2$ AT SATELLITE VELOCITIES

By John W. Boring and Robert H. Humphris



Prepared under Contract No. NASI-2538 by
UNIVERSITY OF VIRGINIA
Charlottesville, Va.

for

NATIONAL AERONAUTICS AND SPACE ADMINISTRATION

# DRAG COEFFICIENTS FOR SPHERES FOR FREE MOLECULAR FLOW IN $N_2$ AT SATELLITE VELOCITIES

Technical Report
under
Contract NASI-2538

Submitted to:

Langley Research Center
National Aeronautics and Space Administration

Submitted by:

John W. Boring
Robert R. Humphris

Division of Aerospace Engineering and Engineering Physics
RESEARCH LABORATORIES FOR THE ENGINEERING SCIENCES
SCHOOL OF ENGINEERING AND APPLIED SCIENCE
UNIVERSITY OF VIRGINIA
CHARLOTTESVILLE, VIRGINIA

Report No. EP-4018-159-69U
February 1969

Copy No. 25

ABSTRACT

Laboratory measurements have been made of the momentum transfer by a beam of $N_2$ molecules to surfaces in the molecular energy range 8-200 eV. The measurements have been performed as a function of angle of incidence for samples of the surfaces of Echo I, Echo II, and Explorer XIX satellites. The results have been used to calculate drag coefficients for spherical bodies, yielding $1.9 < C_D < 2.2$.

TABLE OF CONTENTS


| | Page |
|---|---|
| Abstract | ii |
| List of Illustrations | iv |
| Introduction | 1 |
| Experimental Method | 4 |
| Results | 15 |
| Drag Coefficients | 23 |
| REferences | 32 |

LIST OF ILLUSTRATIONS


| | | PAGE |
|---|---|---|
| Figure 1. | Schematic Diagram of Apparatus . . . . . | 5 |
| Figure 2. | Torsion Balance. . . . . | 8 |
| Figure 3. | Photomicrographs of Surfaces . . . . . | 16 |
| Figure 4. | Momentum Transfer Results for Echo I . . . . . | 17 |
| Figure 5. | Momentum Transfer Results for Echo II. . . . . | 18 |
| Figure 6. | Momentum Transfer Results for Explorer XIX (lines vertical). . . . . | 19 |
| Figure 7. | Momentum Transfer Results for Explorer XIX (lines horizontal). . . . . | 20 |
| Figure 8. | Typical Results as a Function of $\cos\theta$. . . . . | 24 |
| Figure 9. | Drag Coefficient for Echo I. . . . . | 25 |
| Figure 10. | Drag Coefficient for Echo II . . . . . | 26 |
| Figure 11. | Drag Coefficient for Explorer XIX. . . . . | 27 |
| Figure 12. | Average Drag Coefficients. . . . . | 29 |
| Figure 13. | Photomicrograph of Painted Surface. . . . . | 31 |

# INTRODUCTION

One method of investigating the density of the earth's upper atmosphere is by observing the orbital decay of satellites. From a knowledge of the orbital parameters as a function of time one can infer the drag force produced by the atmosphere and hence it is possible to calculate the atmospheric density if the drag coefficient is known. For the free-molecular flow conditions that exist for satellites in the upper atmosphere, a knowledge of the drag coefficient is equivalent to knowing the atmospheric composition and the manner in which individual molecules exchange momentum with the satellite surface. There is, however, very little experimental information available concerning molecule-surface interactions for relative velocities in the satellite range, and a consequent uncertainty in any corresponding theoretical calculations.

In April 1963 the University of Virginia began a program to study in the laboratory the transfer of momentum from atmospheric molecules to solid surfaces, especially for relative velocities in the satellite range and for surfaces that are samples of actual satellite material. The program has been sponsored by NASA, Langley under Contract NASI-2538, with technical cognizance in the Space Vehicle Branch and Space Vacuum Laboratory. The original proposal[1] describes the general approach used, and earlier reports have described the system developed to make the measurements,[2] preliminary results for $N_2$ molecules on several surfaces,[3] and a study of various methods for producing a monatomic oxygen beam.[4] The present report describes the final momentum transfer results for $N_2$ on surfaces of Echo I, Echo II, and unpainted Explorer XIX satellite material, along with calculation of the corresponding drag coefficients for spherical satellites. It was originally intended that measurements would also be made for several satellite surfaces which were painted with epoxy paint, but it was found that these electrically insulating surfaces could not successfully be employed with the present technique, since small electrical charges on these surfaces

produced forces that tended to obscure the small forces that were to be measured. A brief discussion of estimated drag coefficients for the painted surfaces is given in the final section of this report.

Consider now the drag on a satellite moving through a rarefied atmosphere (free molecular flow) with a speed large compared to the thermal motion of the atmospheric molecules. The drag coefficient can then be expressed as[3]

$$C_D = \frac{F}{\frac{1}{2}A\rho v_o^2} = 2\left[1 + \frac{1}{A}\int_s \frac{P_m}{P_o}\cos\theta da\right] \qquad (1)$$

where F is the drag force, A is the cross sectional area of the satellite projected on the plane normal to the direction of motion, $\rho$ is the atmospheric density, $v_o$ is the relative velocity of the satellite through the atmosphere, $P_o$ is the corresponding molecular momentum, $P_m$ is the average component of momentum of reflected molecules along the direction of motion (taken positive when opposite to $P_o$), $\theta$ is the angle of incidence of molecules (measured from the normal to the surface) striking an element of surface da, and the integral extends over the surface of the satellite. The above expression may therefore be used to calculate the drag coefficient for a body of convex shape (so that double reflections are not possible) moving through a one-component atmosphere if the ratio $P_m/P_o$ is known as a function of $\theta$ for a given $v_o$. If the atmosphere contains several components, then it is necessary to know $P_m/P_o$ for each molecular species as well as the proportion of each present. To take a simple example, if one considers a flat plate moving so that its surface is normal to the direction of motion, then $\theta = 0$ for the entire surface and we get

$$C_D = 2\left(1 + \frac{P_m}{P_o}\right) \quad \text{(Flat Plate)}$$

If the momentum of the reflected molecules is small compared to the incident momentum ($P_m/P_o \ll 1$) then $C_D \simeq 2$, whereas if the molecules are reflected back along

the direction of $v_o$ (specularly) with a speed equal to $v_o$, then $P_m = P_o$ and $C_D = 4$. One, therefore, would expect the measured value of $C_D$ for a flat plate to be somewhere between these limits: $2 < C_D < 4$. For a convex body it is conceivable that for a considerable fraction of the surface $P_m$ is in the same direction as $P_o$ and hence is negative, leading to the possibility of values of $C_D$ less than 2.

The present paper is concerned with the measurement in the laboratory of $P_m/P_o$ as a function of $v_o$ and $\theta$ for $N_2$ molecules incident on several surfaces, and the calculation of drag coefficients from the results of these measurements. These drag coefficients should be valid for the situation of a body moving through a rarefied, stationary gas of $N_2$ for surface conditions equivalent to those in the experimental system. It is anticipated that future measurements with the developed system will be concerned with other important upper-atmosphere species such as He and O.

The results of some of the normal incidence measurements were presented at the Sixth International Symposium on Rarefied Gas Dynamics at MIT in July 1968. The more complete results for Echo I and Echo II surfaces are being prepared for publication in the AIAA Journal.

## EXPERIMENTAL METHOD

Most of the techniques employed in making the measurements have been described in previous reports, but they will be briefly given again here for completeness.

The general procedure in measuring $P_m/P_o$ is to produce a beam of molecules having a known energy corresponding to satellite velocities (the energy in the case of $N_2$ molecules is 8-18 eV), allow the molecules to strike a test surface at a chosen angle of incidence, and measure the component of force on the test surface along the beam direction. If the rate at which the molecules strike the surface (mol./sec.) is determined, then the force divided by the rate gives $(P_o + P_m)$, and since $P_o$ is already known from a knowledge of the energy and mass of the beam molecules, then one has sufficient information to determine $P_m/P_o$.

A schematic drawing of the entire experimental system is shown in Figure 1. The apparatus is mounted in two separate vacuum chamgers, a beam chamber and a test chamber. The beam chamber contains the ion source, electrostatic lens system, neutralization cell, and electrostatic collection plates. The test chamber contains the test surface which is mounted on a torsion balance used to measure the force produced by the beam on the surface. The test chamber is placed on a large concrete pier which is isolated from the laboratory floor to reduce mechanical vibrations in the torsion balance. The two chambers are connected by a metal bellows which allows movement of the beam chamber so that the beam can be moved with respect to the test surface. The vacuum chambers are pumped continuously by diffusion pumps, but the principal pumping during operation is provided by a 6600 l/sec. cryopanel which is cooled to 20°K by a Malaker Cryomite mechanical refrigerator, providing an operating pressure in the beam chamber of $2\text{-}4 \times 10^{-7}$ Torr.

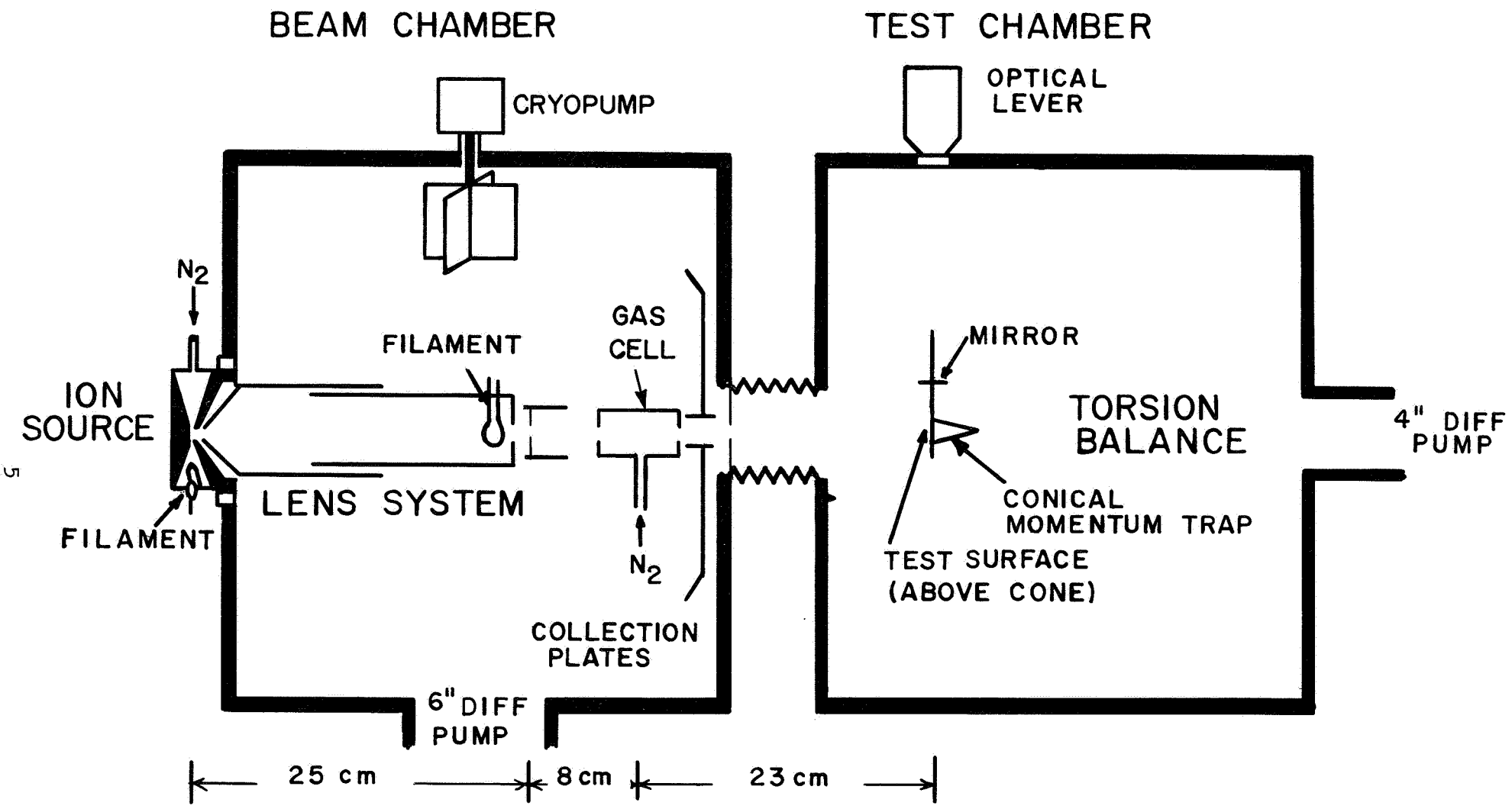


Figure 1. Schematic Diagram of Apparatus

The ion source and lens system are patterned after the design of Utterback and Miller,[5] but larger apertures are used to increase the usable ion currents. The pressure in the ion source is typically 20 microns and the anode current is around 10 ma at an anode voltage of 30V. The ion beam is extracted from the ion source through a 0.44 mm diameter hole by an extraction potential of 250V.

It has been suggested[6] that the space charge spreading of an ion beam could be minimized by injecting electrons into the beam to make the composite beam macroscopically neutral. For the beam described here the ion density is of the order $10^6$ ions/cm$^3$ so the recombination[7] between the $N_2^+$ ions and free electrons of an equal density is not expected to be significant. The electron injection is accomplished here by placing just before the third lens a circular 0.20 mm tungsten filament 1.5 cm in diameter, the axis of the circle being along the beam axis. Some of the electrons are formed into a beam by the field of the third lens and the attraction of the positive space charge of the ion beam. The composite beam of $N_2^+$ ions and electrons passes on through the third lens to the neutralization cell. The assertion that there is negligible recombination between the electrons and ions was checked experimentally by observing that no neutral beam was detected when the neutralizing gas was removed. For a 10 eV $N_2^+$ beam, the maximum ion current transmitted through the neutralizing cell was found to be around $10^{-9}$ amp when no electrons were injected into the beam, and was $4 \times 10^{-8}$ amp ($\sim 2 \times 10^{11}$ ions/sec) when the electron current in the composite beam was approximately $2 \times 10^{-7}$ amp.

The beam leaving the neutralization cell is composed of $N_2^+$ ions that were not neutralized, neutralized $N_2$ molecules, electrons, and some low-energy $N_2$ molecules from the neutralizing gas. The charged particles are removed from the beam by a transverse electric field created by two parallel plates.

The torsion balance which is used to measure the force produced by the beam on the test surface was patterned after one described by Pearson and

Wadsworth[8] and uses electrostatic damping and an optical lever[9] for measuring the angular deflection of the balance arm. This balance is relatively rugged but is capable of detecting forces as small as $2 \times 10^{-8}$ dyne. The balance configuration used in our work is shown in Figure 2. The torsion fiber is 10 micron tungsten, and both damping plates are mounted on the same end of the balance arm. The test surface is mounted on the other end of the balance arm along with a momentum trap for measuring the beam flux. The procedure is to allow the beam to enter the momentum trap, measure the balance deflection, and calculate the beam flux under the assumption that the molecules leaving the trap have a Maxwellian velocity distribution which is characteristic of the temperature of the trap. (The results are not very sensitive to the precise validity of this assumption since the average momentum of nearly thermally accommodated molecules leaving the trap is much less than that of the incident molecules.) The beam is then moved upward mechanically so that it strikes the test surface and the balance deflection is again observed, giving the force produced by the beam. This method of measuring the beam flux has the advantage that the absolute calibration of the balance is not needed, since two balance deflections are being compared in order to find the average momentum transferred to the test surface by the molecules of the beam. In each measurement the ion beam is turned on and off and the resulting balance deflection is taken as a measure of the force of interest. The effect of all forces on the balance other than that produced by the beam (such as that caused by the neutralizing gas) are thus eliminated. The momentum trap is 4.1 cm long with an apex angle of 22° and with a 0.9 cm diameter hole. The ratio of the hole area to the total internal surface area of the cone is 0.052, so that one would expect entering molecules to experience, on the average, around 20 collisions with the surface of the box before leaving. This means that if one assumes that the thermal accommodation coefficient for a single collision of a molecule with the inner surface of the cone is greater than around 0.2, the assumption that the molecules leaving the box have an average velocity that is characteristic of the box temperature is well satisfied. Although there

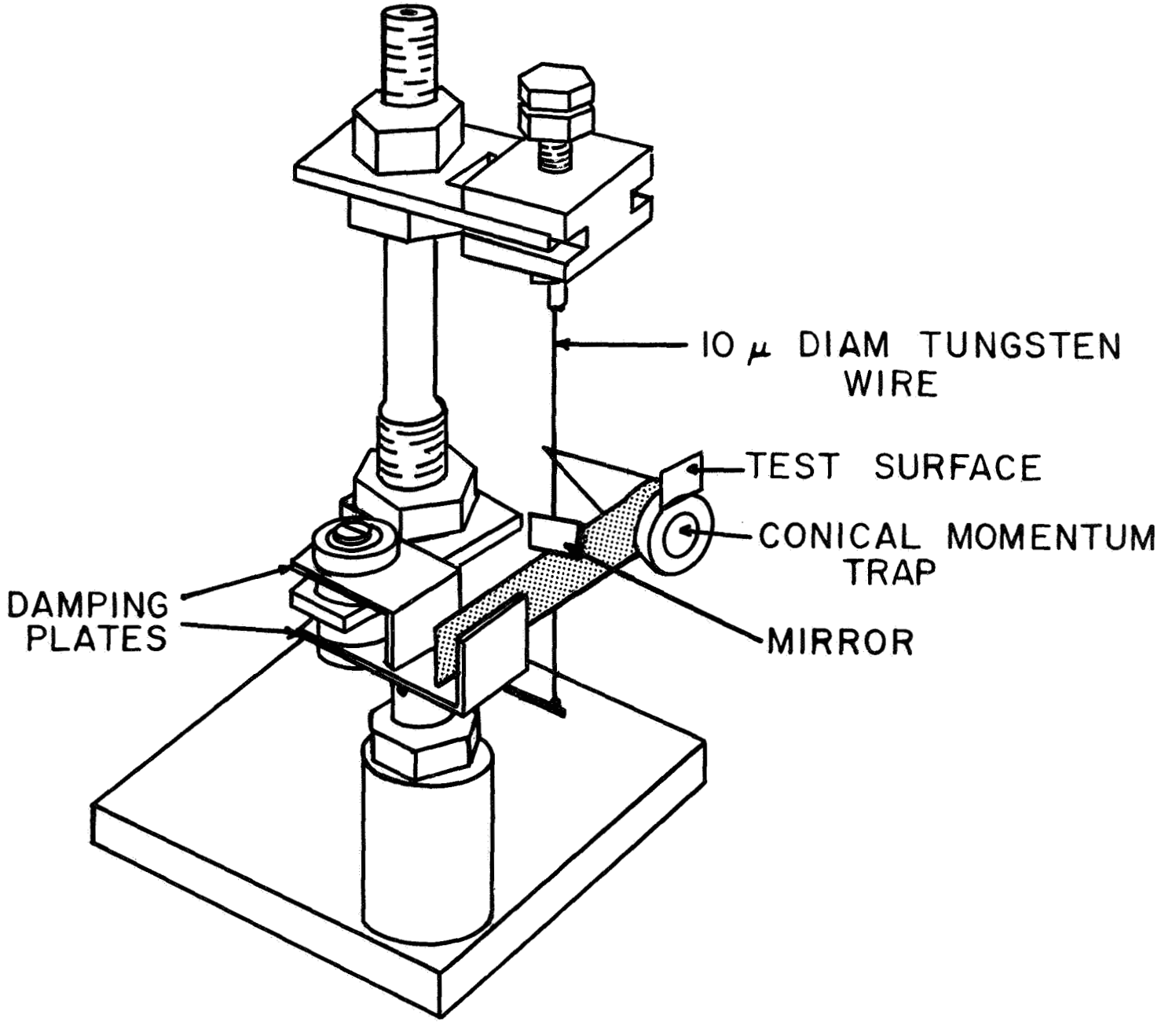


Figure 2. Torsion Balance

have been no measurements of the accommodation coefficient in the eV energy range, the measurements at thermal energies[10] indicate that for gas covered surfaces the accommodation coefficient is generally greater than 0.5. Theoretical consideration of the particle-surface interaction as being hard-sphere at eV energies also leads one to think that the accommodation coefficient for these studies (with or without adsorbed gases) will be in excess of 0.5. All measurements described here were performed with test surfaces at room temperature.

As stated earlier, the principal difficulty in using the electrical acceleration method, described in the previous sections, is in achieving an adequate beam flux for detection by the torsion balance. One is concerned, then, with a signal-to-noise problem where the signal is the force produced by the beam on the test surface and the noise is that of the torsion balance. As an example of the magnitudes involved for a 10 eV $N_2$ beam with a flux of $10^{11}$ mol/sec, the force produced on the test surface would be $3.8 \times 10^{-6}$ dyne, under the assumption that the reflected molecules carry away negligible momentum. If the reflected molecules have appreciable momentum compared to the incident momentum, the force would then be larger. The minimum measured rms noise of this type of torsion balance is around $2 \times 10^{-8}$ dyne[8], and this figure is just about equal to what one expects for the Brownian motion of the balance vane. The following paragraphs contain descriptions of the measured characteristics of the present system.

The beam characteristics given here will be for a $N_2$ beam with an energy of 10 eV. For higher energies the usable beam flux will be greater, while for lower energies it will be less. The other characteristics of the beam generally will not depend on the beam energy. A typical set of characteristics for the beam system is given below.

| | 10 eV $N_2$ Beam |
|---|---|
| $N_2^+$ Current Extracted from Ion Source | $5 \times 10^{-7}$ amp |
| $N_2^+$ Current Through Empty Neutralizing Cell | $4 \times 10^{-8}$ amp |

| | |
|---|---|
| Electron Current Through Neutralizing Cell | $2 \times 10^{-7}$ amp |
| Percent Neutralization of $N_2^+$ | 20% |
| $N_2$ Beam Striking Test Surface | $4 \times 10^{10}$ mol./sec. |
| Force Produced on Test Surface by Beam | $1.5 \times 10^{-6}$ dyne |
| Energy Spread of Beam | ±0.5 eV |
| Diameter of Beam at Test Surface | 0.6 cm |

Measurements can be made easily with this beam system at any beam energy greater than 10 eV, since larger beam fluxes are obtainable at the higher energies. The system can be used to extend the measurements to atomic and molecular species other than $N_2$. However, separate studies need to be made to achieve suitable operation of the system for each species.

The most important characteristic of the balance is its noise level expressed in force units. The period of the balance in its torsional mode is also a consideration since this determines the length of time required for oscillations to be damped out after the beam is allowed to deflect the balance. It is also desirable to have the balance reasonably rugged so that a minimum amount of time is spent in construction and testing of each new balance.

With a 10 micron tungsten torsion fiber the balance is sturdy enough to be constructed without special equipment and can be handled easily. A typical rms noise level in angular units for this balance is around $4 \times 10^{-7}$ radians, or, expressed in units of force, it is $4 \times 10^{-8}$ dynes. At times of minimum external disturbance, the noise level of the balance was found to be about equal to the Brownian limit of $2 \times 10^{-8}$ dyne. The larger noise values result from pressure variations due to the irregular pumping characteristics of the diffusion pumps and from vibrations reaching the balance. The torsional period of the balance depends on the moment of inertia of the vane assembly which is slightly different for each new balance but a typical value for the period is 15 seconds.

In a measurement the beam is allowed to strike the test surface and the balance deflection is recorded. The beam chamber is then moved downward

mechanically so that the beam enters the momentum trap, and the corresponding balance deflection is recorded. The ratio of these two deflections then gives

$$R = \frac{P_o + P_m}{P_o + P_a} ,$$

where $P_a$ is the momentum due to the molecules leaving the momentum trap and has a maximum value for these experiments of around 0.055 $P_o$. If one assumes that the molecules collide with the walls of the momentum trap a sufficiently large number of times that they are in thermal equilibrium with the walls and leave with a corresponding velocity and angular distribution, then by knowing the temperature of the walls, $P_a$ can be calculated, and

$\frac{P_m}{P_o}$ can be easily computed from

$$\frac{P_m}{P_o} = R\left(1 + \frac{P_a}{P_o}\right) - 1.$$

In the measurements to be discussed in the next section the neutralization cell is located about 18 cm from the test surface on the torsion balance. This allows a considerable distance within which the neutral beam can diverge appreciably, especially at the low energies where the ion beam before neutralization is expected to be rather divergent. The diameter of the beam at the test surface at low energies was found to be around 1 - 1.5 cm. Since it is difficult to construct a satisfactory balance with the test surface and the entrance aperture of the momentum trap as large as this, some means was necessary to collimate the neutral beam before it reached the balance. This was accomplished by placing two 0.6 cm dia. collimating holes, one above the other, just before the balance. The diameter of the holes is such that all of the beam passing through the top hole will strike the test surface and all of the beam passing through

the bottom hole will enter the momentum trap. The measurement is then performed by closing the bottom hole with a shutter, allowing a portion of the beam to pass through the upper hole and strike the test surface, and recording the corresponding balance deflection. The beam chamber is then moved downward a distance equal to the separation between the two holes, the top hole is closed and the bottom one opened, the same portion of the beam is allowed to pass through the bottom hole and enter the momentum trap, and the balance deflection is recorded. The ratio of these two deflections, then, gives the value of R.

Because of the nature of the method used to produce the beam there are forces on the balance in addition to the desired force. This requires that the method used to obtain the balance deflection should eliminate any effects due to these extraneous forces. First, there is a force on the balance produced by $N_2$ gas effusing from the neutralizing cell, which may be considerably larger than that caused by the molecules of interest. Second, there can be a force produced by high energy neutral molecules that were produced by charge transfer of beam ions in the residual gas of the beam chamber at points within the electrostatic focusing system where the ion energy is higher than the desired energy. One must then have a method of obtaining balance deflections which are due only to the desired neutral beam molecules and are not affected by the magnitude of these extraneous forces. This is accomplished by allowing all of these molecules to strike the balance and then measuring the balance deflection that results when the molecules of interest are prevented from reaching the balance. This in effect allows one to ignore the effect of the unwanted molecules. The molecules of interest (which in previous discussion we have called the beam) are prevented from reaching the balance by changing the potential on an electrode just before the neutralization cell so that the ions cannot enter the cell. This eliminates the force on the balance caused by the neutral molecules formed by neutralization of these ions, but does not affect the forces due to the effusing gas molecules and the high energy neutrals. The corresponding balance deflections caused by turning the ion beam on and off

in this manner is then the desired deflection. This procedure is, of course, repeated for both the test surface and the momentum trap.

Generally four or five measurements are taken with the beam striking the test surface, then a similar number with the beam entering the momentum trap, and then another set with the test surface. The average for the test surface is then compared to the average for the momentum trap. The fact that a complete measurement includes two sets for the test surface tends to minimize the effect of slowly changing beam conditions.

The measurements were performed for several different test surfaces. The entire question of surface condition in experiments such as these involves a number of uncertainties. In considering the application of the measurements to satellite studies of the density of the earth's upper atmosphere, one would like to make the measurements using samples of actual satellite surfaces which have the same surface condition as that of the satellite in orbit (especially regarding adsorbed gases on the surface). There are two reasons why this desirability cannot be achieved at present. First, the condition of the satellite's surface is to a large extent unknown. It depends on the preparation of the satellite, its environment in orbit, and possible continual emission of gases from portions of the satellite. Second, even the most advanced laboratory techniques are not presently capable of specifying precisely the condition of a surface under study. It is possible, however, that some aspects of the molecule-surface interaction are not especially sensitive to the exact nature of the surface, particularly aspects that involve averages over a number of parameters. Since the momentum transfer measurements described here provide a rather coarse study of the interaction, the following philosophy has been adopted with regard to surface condition. The measurements are performed for several test surfaces, but the exact condition of the surface is not rigidly controlled. The surfaces are handled carefully before placing them in the vacuum system so as to prevent their being contaminated by oils, fingerprints, etc., but no attempt is made to remove adsorbed gases from the surfaces after they are in the vacuum system and the measurements

are performed at pressures (~ $10^{-6}$ Torr) such that a clean surface (no adsorbed gases ) cannot be maintained. If the results of the measurements indicate that only the gross character of the surface (such as surface roughness) affects the momentum transfer, then one might conclude that the surfaces can be adequately characterized for this particular type of measurement. Measurements that investigate finer details of the interaction, such as the angular and velocity distribution of the reflected particles, may require considerably more accurate surface characterization.

## RESULTS

The objective in these measurements is to investigate $\frac{P_m}{P_o}$ as a function of molecule energy and angle of incidence for several test surfaces, including samples of surfaces used on actual satellites. The surfaces used in these studies were samples of material used in the earth satellites Echo I, Echo II, and Explorer XIX (no paint). Photomicrographs of these three surfaces to show the gross roughness are shown in Figure 3. The results of the measurements are presented in Figures 4-7, in which the ratio $\frac{P_m}{P_o}$ is plotted versus the incident energy $E_o$. The measurements extend up to an energy of 200 eV since these results are rather easily obtained and they indicate the high energy limit of the momentum transfer. One of the principal factors in determining the nature of the particle-surface interaction is the ratio of the masses of the incident molecule and the surface atoms that it strikes. For this reason a measurement was made for a gold surface (mass number 197) at $\theta = 0°$ to see if the results are affected by a large change in the mass number of the base material. The fact that the results for gold were essentially the same as for the other surfaces indicates that under the conditions of these measurements the interaction with adsorbed gases appears to predominate.

A straight-forward investigation of the dependence of the ratio $\frac{P_m}{P_o}$ on the angle of incidence would involve mounting the test surfaces on the balance vane so that the beam molecules strike the surface at the chosen angle, but with the beam direction still perpendicular to balance vane. This means that the balance must be modified or reconstructed for each new angle. At angles of incidence less than 30° this procedure was followed with success. At larger angles, however, it was found that the combination of the mass of the momentum trap and that of the larger test surface needed to intercept all of the beam passing through the collimating aperture caused the balance to be intolerably noisy. Since all the surfaces studied gave essentially identical results it was decided that the measurements

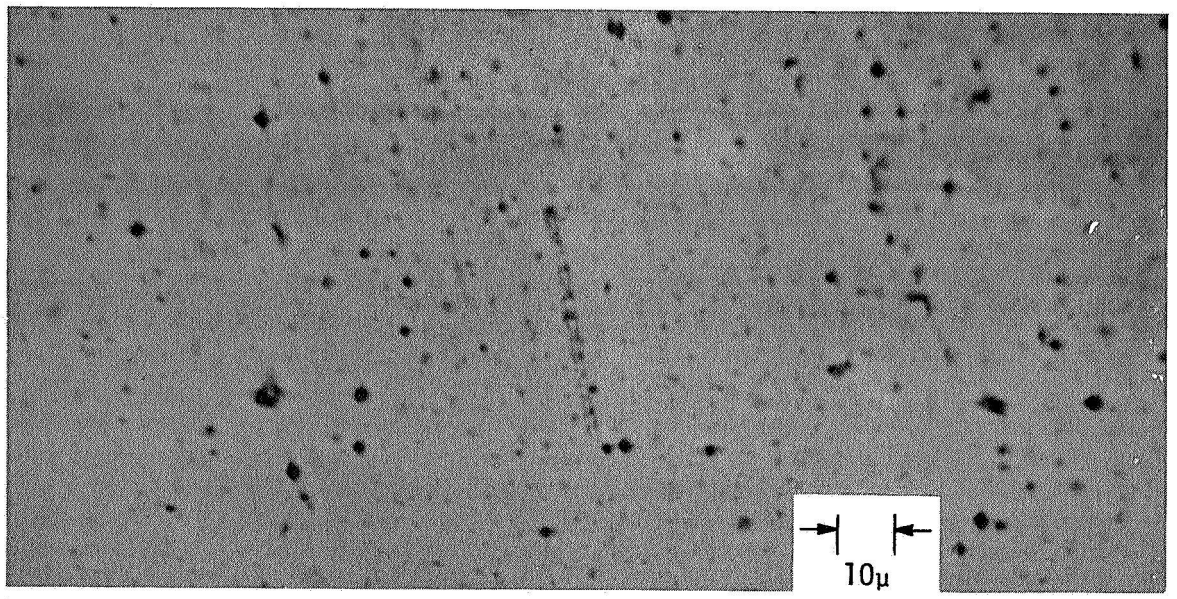


Echo I

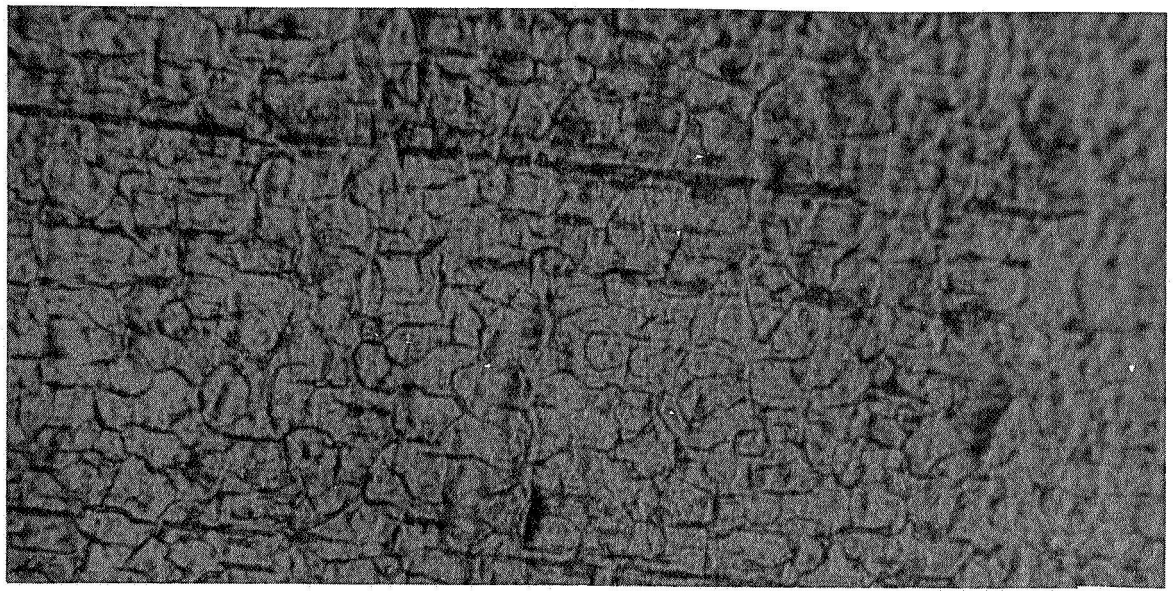

Echo II

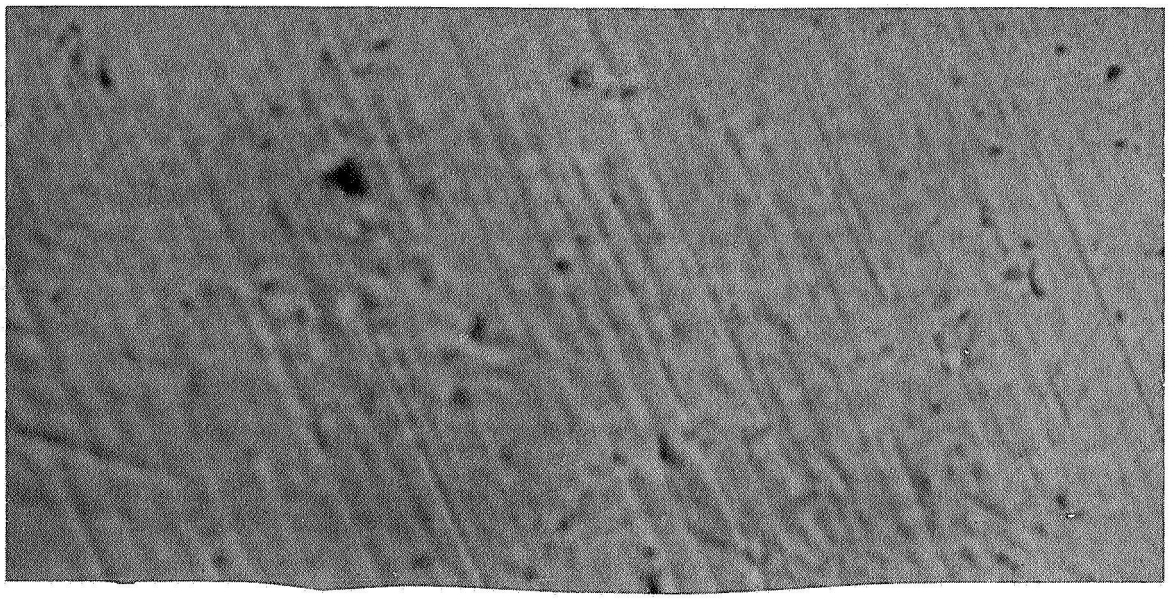

Explorer XIX
(no paint)

Figure 3. Photomicrographs of Surfaces

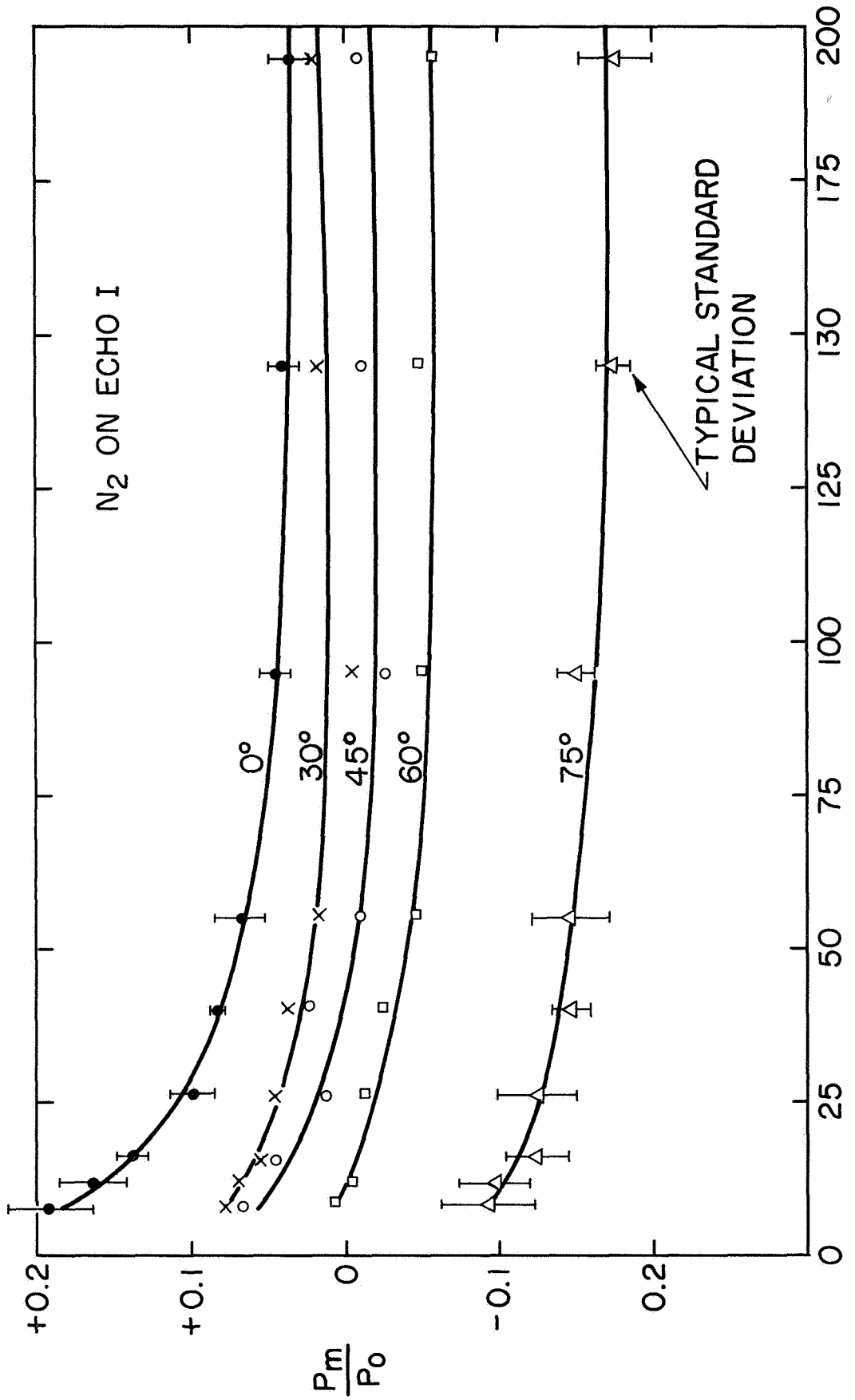


Figure 4. Momentum Transfer Results for Echo I

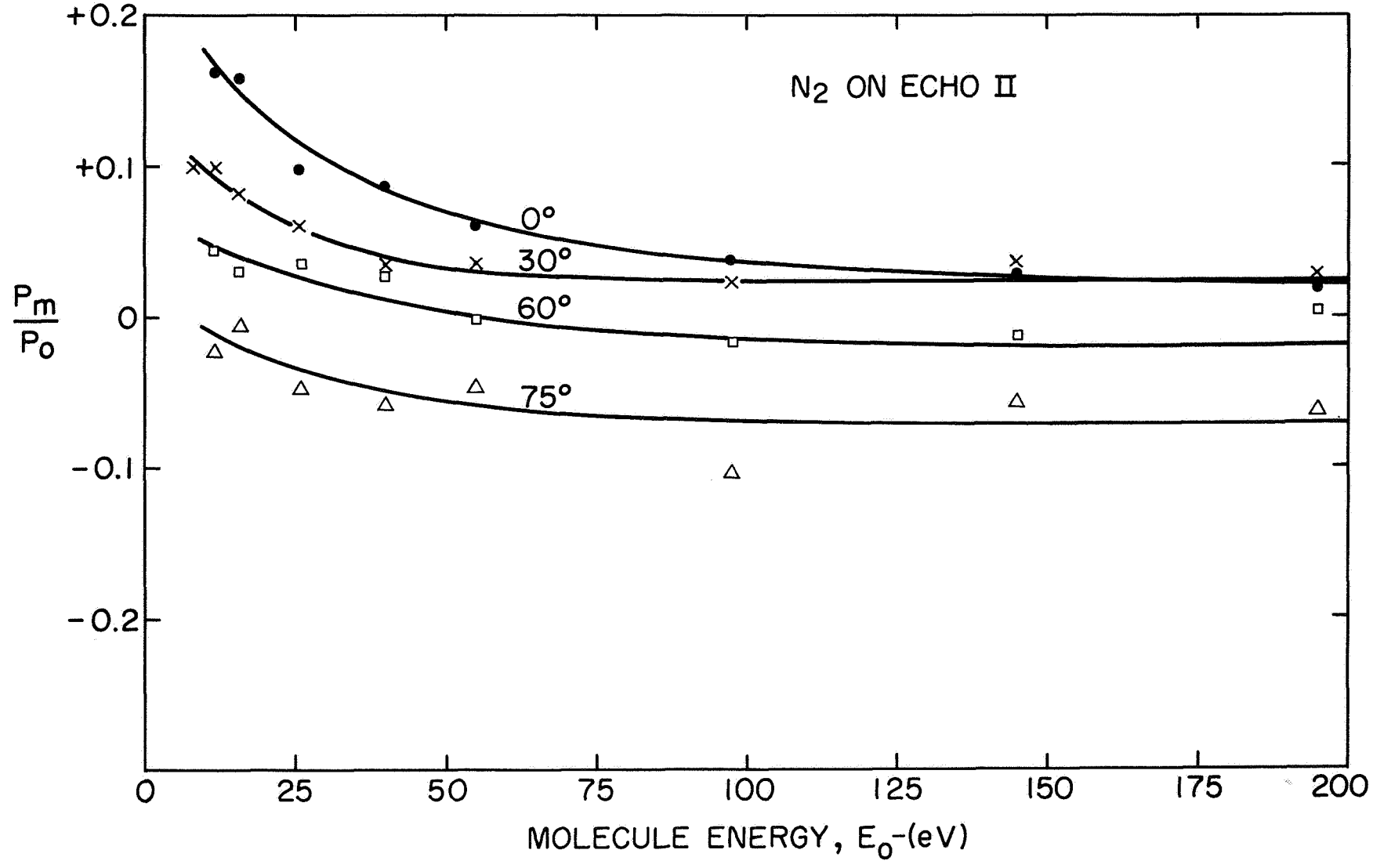


Figure 5. Momentum Transfer Results for Echo II

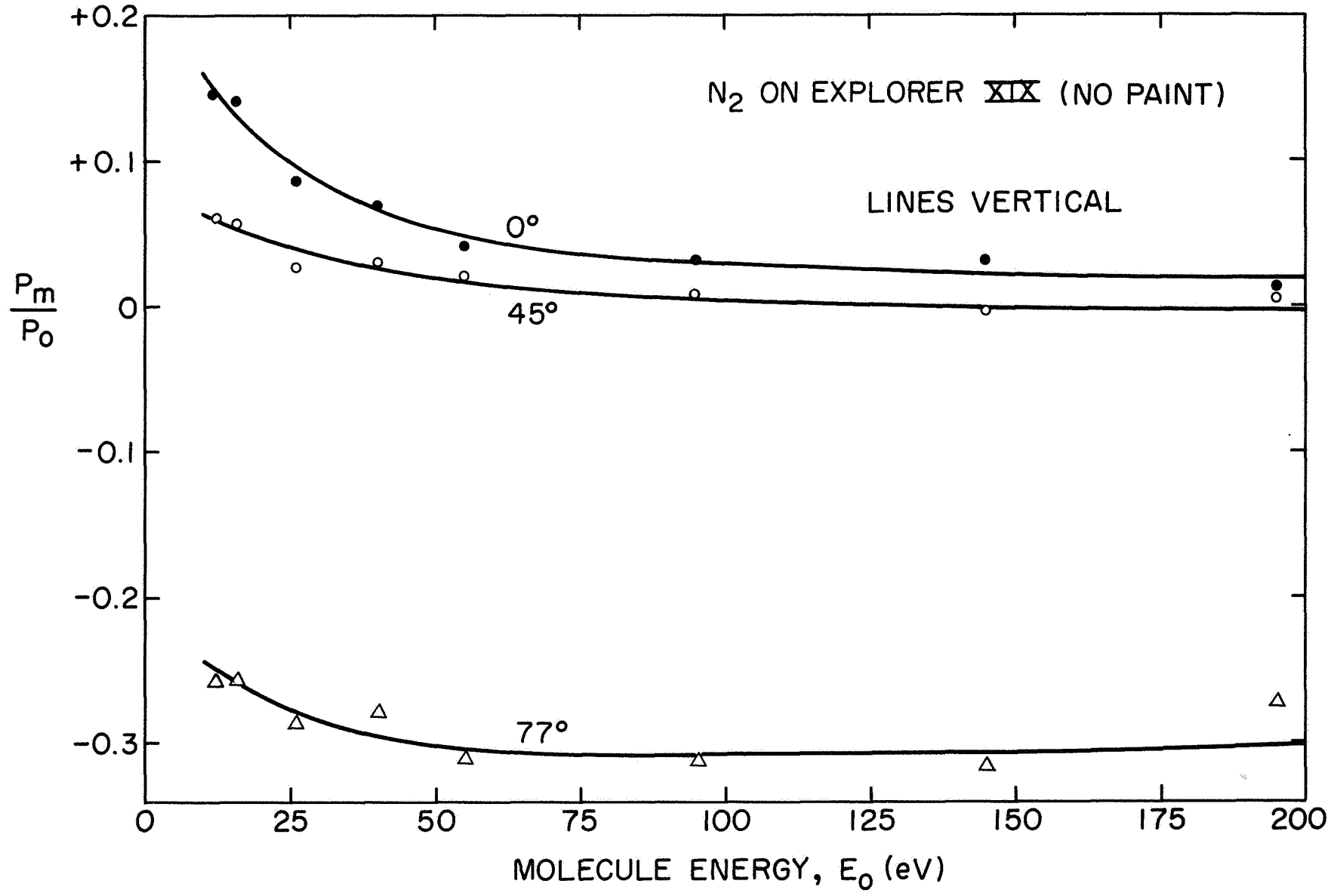


Figure 6. Momentum Transfer Results for Explorer XIX (lines vertical)

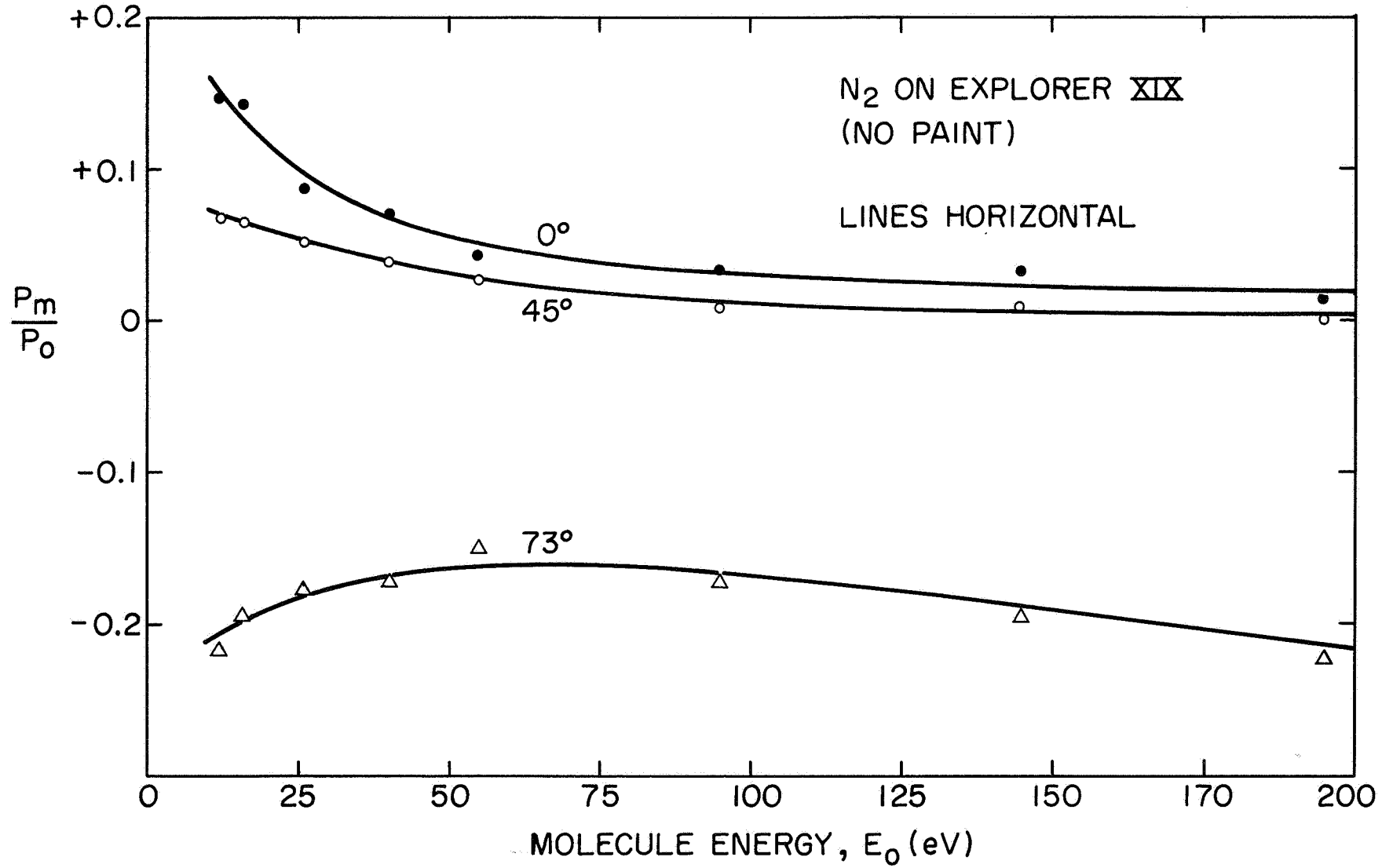


Figure 7. Momentum Transfer Results for Explorer XIX (lines horizontal)

at larger angles would be performed by eliminating the momentum trap and using one of the surfaces studied earlier (at $\theta = 0°$) as a reference surface, thereby reducing the mass mounted on the balance arm. The ratio $\frac{P_m}{P_o}$ for the larger angles can thus be obtained by comparing deflections for the inclined surface and the reference surface, and then using the results obtained previously which provided a comparison of the reference surface with the momentum absorber. If the deflection for the inclined surface divided by the deflection for the reference surface is called S, then

$$S = \frac{P_o + P_m}{P_o + P_m^o} = \frac{1 + \frac{P_m}{P_o}}{1 + \frac{P_m^o}{P_o}} ,$$

where $P_m^o$ is the value of $P_m$ for the reference surface for $\theta = 0$. Also,

$$R^o = \frac{P_o + P_m^o}{P_o + P_a} = \frac{1 + \frac{P_m^o}{P_o}}{1 + \frac{P_a}{P_o}} ,$$

where $R^o$ is the value of R for the reference surface at $\theta = 0$. Eliminating $\frac{P_m^o}{P_o}$ between the expressions for S and $R^o$ and solving for $\frac{P_m}{P_o}$ one gets

$$\frac{P_m}{P_o} = S\, R^o \left(1 + \frac{P_a}{P_o}\right) - 1.$$

This is the expression used for obtaining $\frac{P_m}{P_o}$ for the larger angles of incidence where one is comparing the force on an inclined surface to that on a reference surface.

In Figure 4 for the Echo I surface error bars are shown for the measurements at $\theta = 0°$ and $\theta = 75°$, and are representative of the corresponding uncertainties in the other measurements. The error bars give the standard deviation in the mean value of $\frac{P_m}{P_o}$ as calculated from a number of measurements at a given energy, and therefore represent the result of random fluctuations from the mean value caused by system noise, etc. No inclusion has been made of possible systematic errors in the measurements, but it is felt that these should be small since the measurements involve a comparison of two determinations of the same type of quantity (balance deflection) which were repeated a number of times for each surface and angle over a period of several months.

It is seen in the photomicrograph of the Explorer XIX surface in Figure 3 that there is a pattern of parallel grooves and ridges. It was found that for the measurements of $\frac{P_m}{P_o}$ for this surface at the larger angles, the orientation of this pattern affected the results. The measurements shown in Figure 6 for 45° and 75° were taken with the grooves vertical (projection of the grooves on the normal to the beam direction is vertical), while those of Figure 7 were taken with the grooves horizontal. The behavior of the $\theta = 75°$ curve in Figure 7 at low energies is unusual in that $\frac{P_m}{P_o}$ decreases with decreasing energy. These low energy measurements were repeated a number of times to check the results, and the dependence shown in Figure 7 was obtained consistently.

## DRAG COEFFICIENTS

One of the purposes of these measurements has been to allow one to calculate drag coefficients for bodies moving in free-molecular flow with speeds in the satellite range. With the experimental results of the last section and Equation (1) one can calculate drag coefficients for a body of any convex shape. In this section such calculations for spherical bodies are performed.

In order to do the integration indicated in Equation (1) over a sphere it is necessary to know $\frac{P_m}{P_o}$ as a function of $\theta$. Figure 8 shows a typical plot of $\frac{P_m}{P_o}$ versus $\cos\theta$ taken from Figures 4-7 for two energies. For a sphere Equation (1) can be written as

$$C_D = 2\left[1 + 2\int_0^{\frac{\pi}{2}} \frac{P_m}{P_o} \sin\theta\cos\theta d\theta\right] \qquad (2)$$

Taking the data points of Figure 8 and fitting them with straight line segments (three or less) in the range $0.26 \leq \theta \leq 1.00$ one can easily calculate the contribution to the drag coefficient for parts of the sphere where $\theta$ is less than 75°. Since no data was taken for angles greater than 75°, then some extrapolation to larger angles must be used. Consider two such extrapolation procedures as bounds on the actual behavior of the curve in this region: (1) an extension of the straight line segment used for angles slightly less than 75° to angles $75° \leq \theta \leq 90°$ will give the upper bound to the actual curve and (2) a straight line drawn from the data point at 75° to $\frac{P_m}{P_o} = -1$ at $\theta = 90°$ will give the lower bound. Plots of the drag coefficients obtained by these two methods are shown in Figures 9-11. It is seen that the two extremes in extrapolation amount to about a ± 1 percent difference in the value of the drag coefficient.

In Figure 12 the curves of drag coefficient versus energy have been plotted for the three surfaces Echo I, Echo II, and Explorer XIX. These represent averages of the two limiting extrapolation procedures, and for

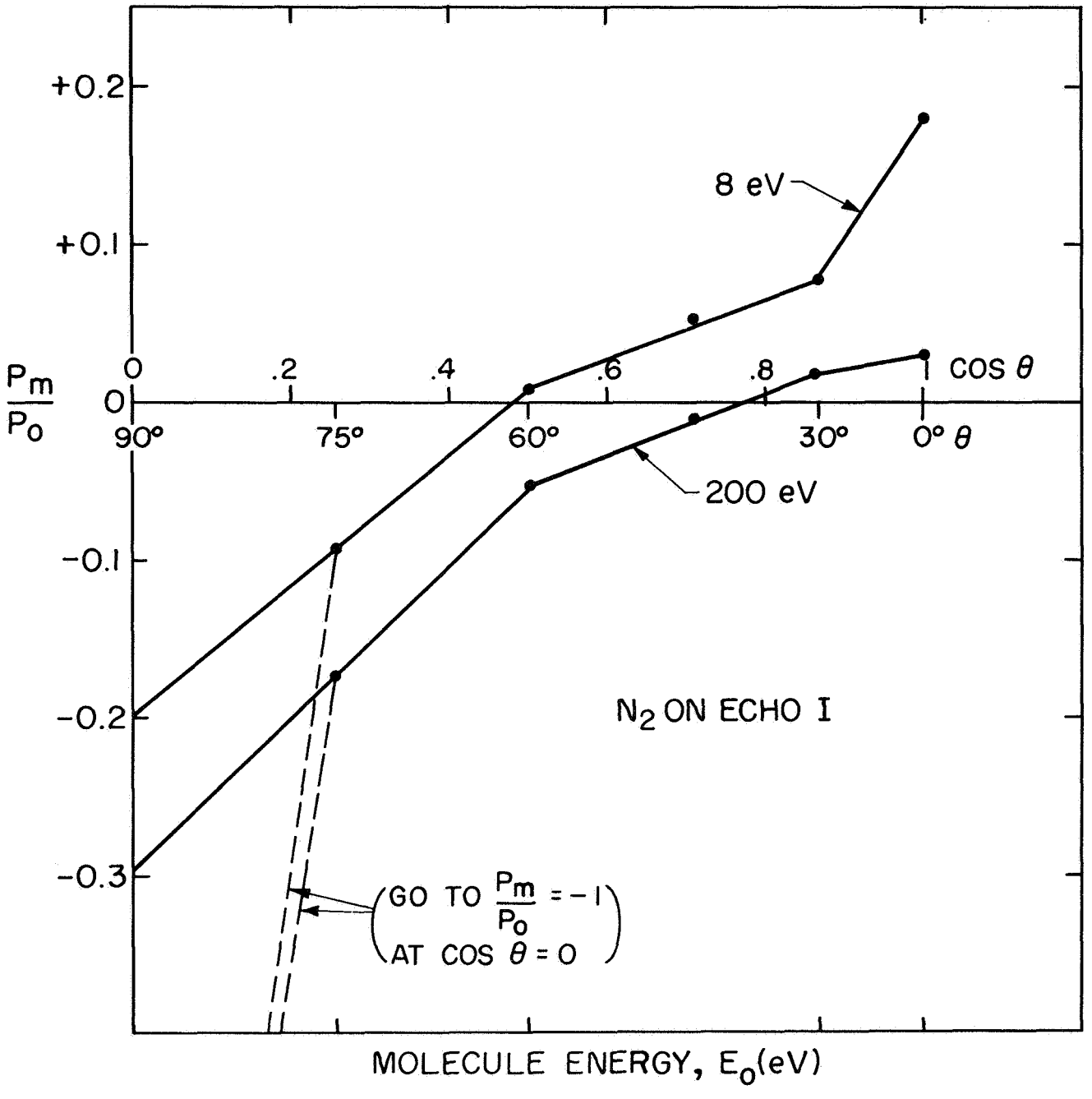


Figure 8. Typical Results as a Function of cosθ

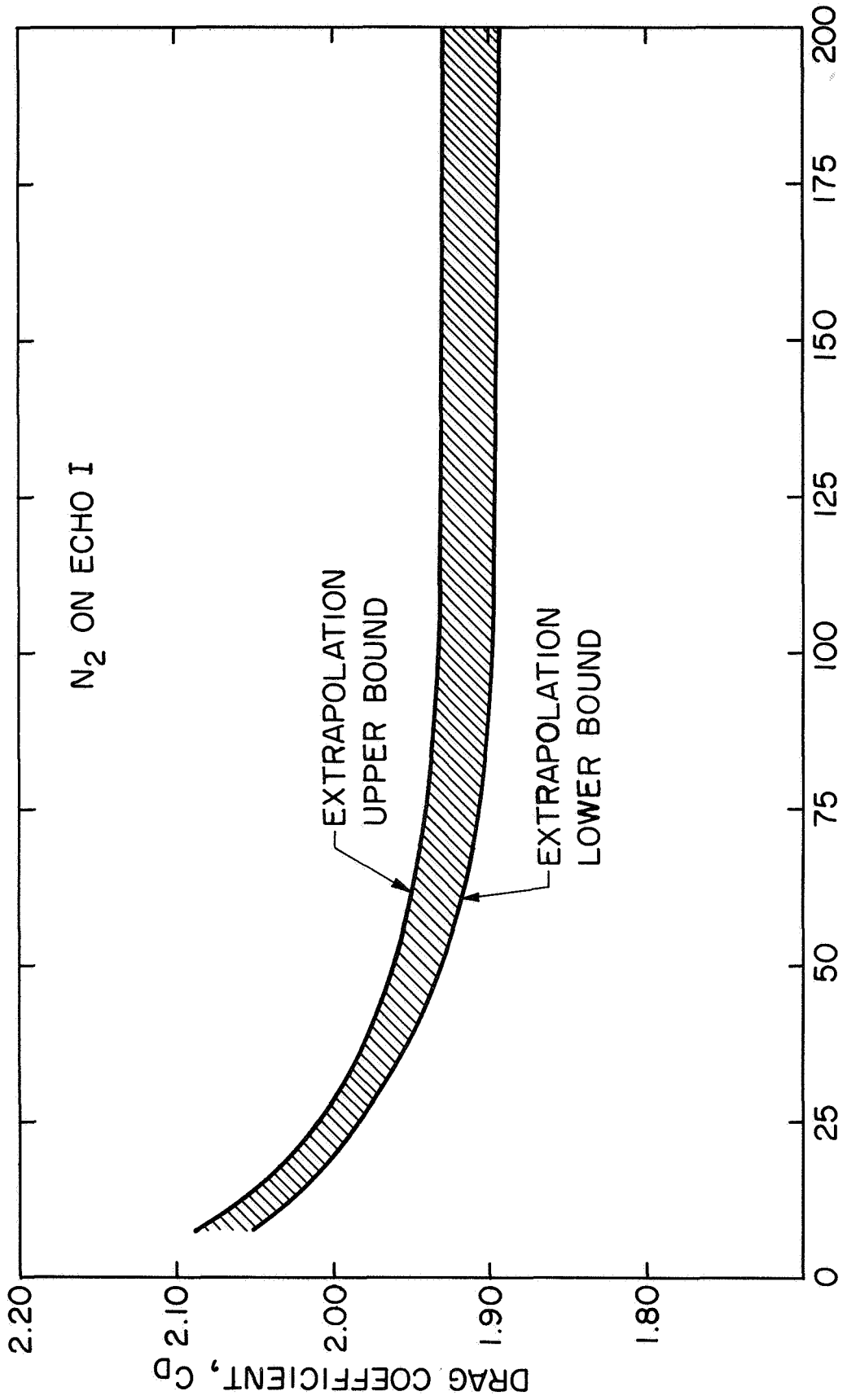


Figure 9. Drag Coefficient for Echo I

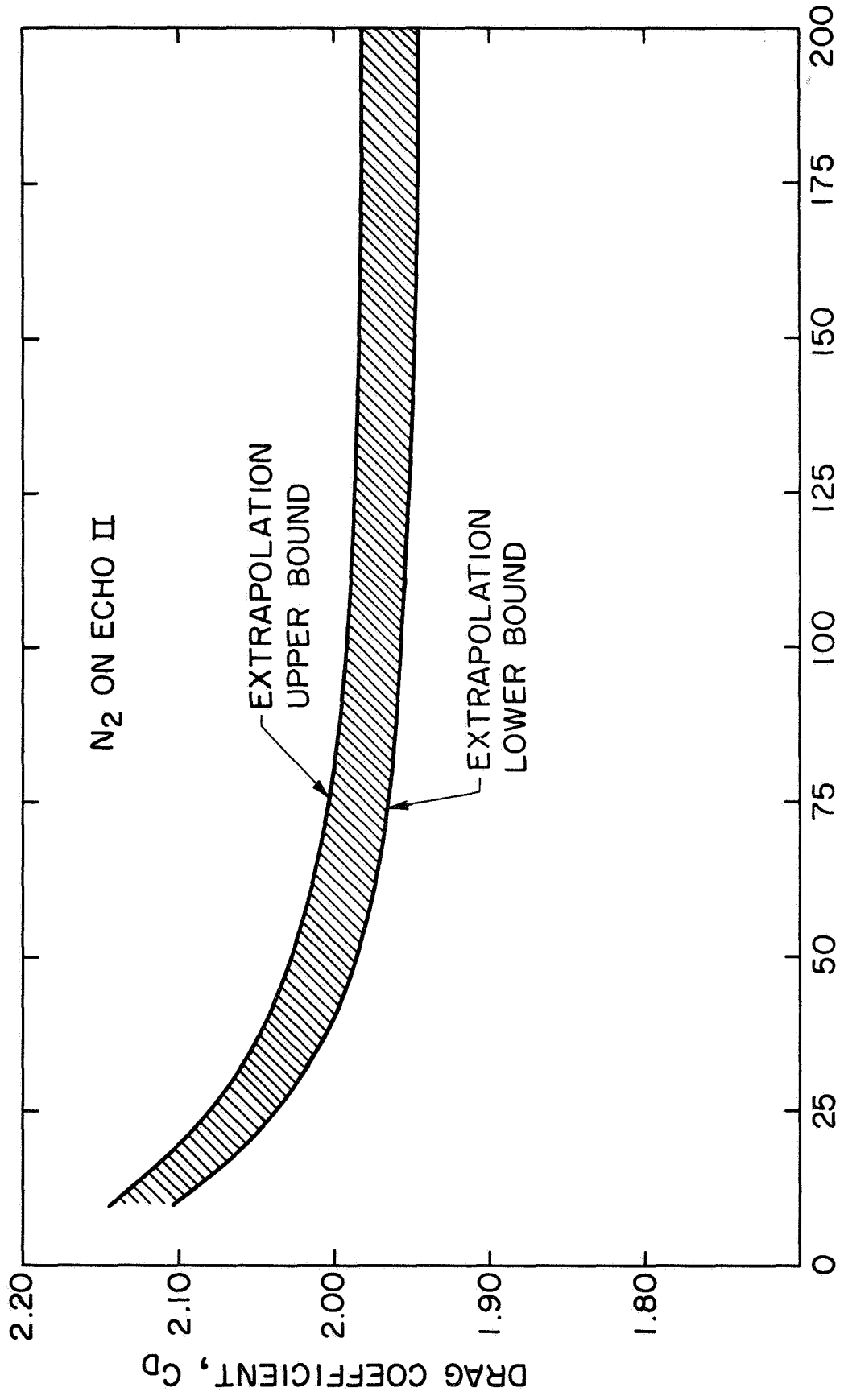


Figure 10. Drag Coefficient for Echo II

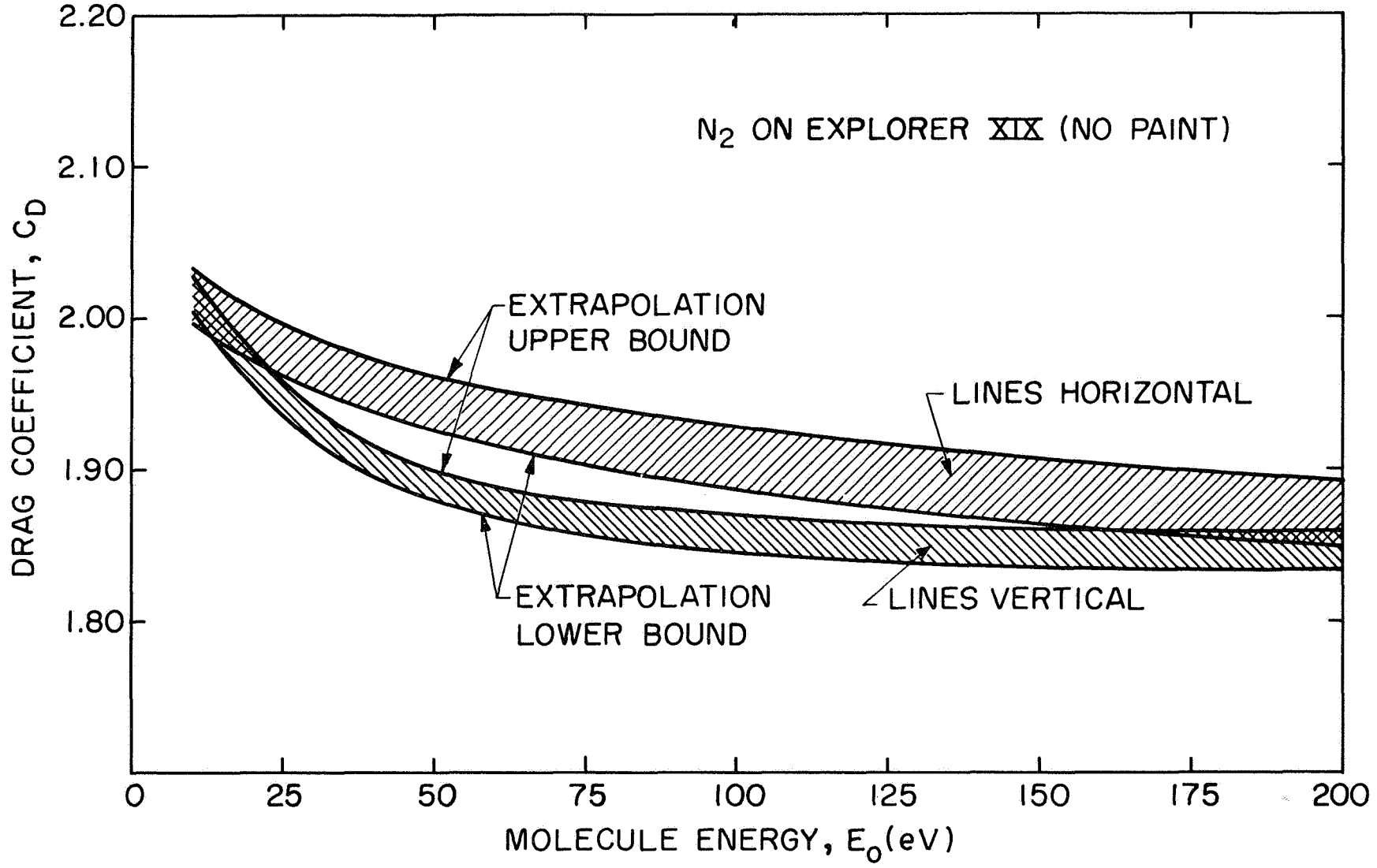


Figure 11. Drag Coefficient for Explorer XIX

the case of Explorer XIX an average also of the two orientations of surface grooves (or lines). It is seen in Figure 12 that for a given energy (or velocity) the value of $C_D$ varies by about 6 percent from the surface with the minimum value (Explorer XIX) to the one with the maximum value (Echo II). A large part of this variation is probably attributable to differences in gross surface roughness. In Figure 3 it is seen that the Echo II surface has a large number of rather sharp cracks which would be expected to lead to larger values of $P_m$ than for a smoother surface, and hence to larger values of $C_D$. The surface of the Echo I sample appears rather smooth with a few relatively small irregularities. The Explorer XIX surface which is rolled aluminum foil, shows the grooves mentioned earlier but the depressions appear deeper and more rounded than the crack structure seen in the Echo II surface.

The error bars on the low energy data (shown typically in Figure 4) would lead to about a ± 1 percent uncertainty in the drag coefficient, which along with the uncertainty in the large angle extrapolation procedure would lead to a total uncertainty in the drag coefficients of about 2 percent for the lowest energies of the curves of Figure 12.

Consider now the question of estimating drag coefficients for surfaces other than those for which measurements were described above. From the fact that the $\theta = 0°$ results seem rather insensitive to both the base material of the surface and the gross surface roughness, the variation in value of drag coefficient seen for the three surfaces in Figure 12 comes about mainly due to the different large angle behavior of the results. It is very likely that surface contour differences are what lead to this behavior, although the distance scale on which these contour differences are most important is not known. A good guess for an unknown surface might be to take a photomicrograph of the surface and compare it to those of Figure 3. If the surface looked rather smooth or had large rounded irregularities one might expect that the corresponding drag coefficient would fall somewhere between the curves for Echo I and Explorer XIX, whereas if

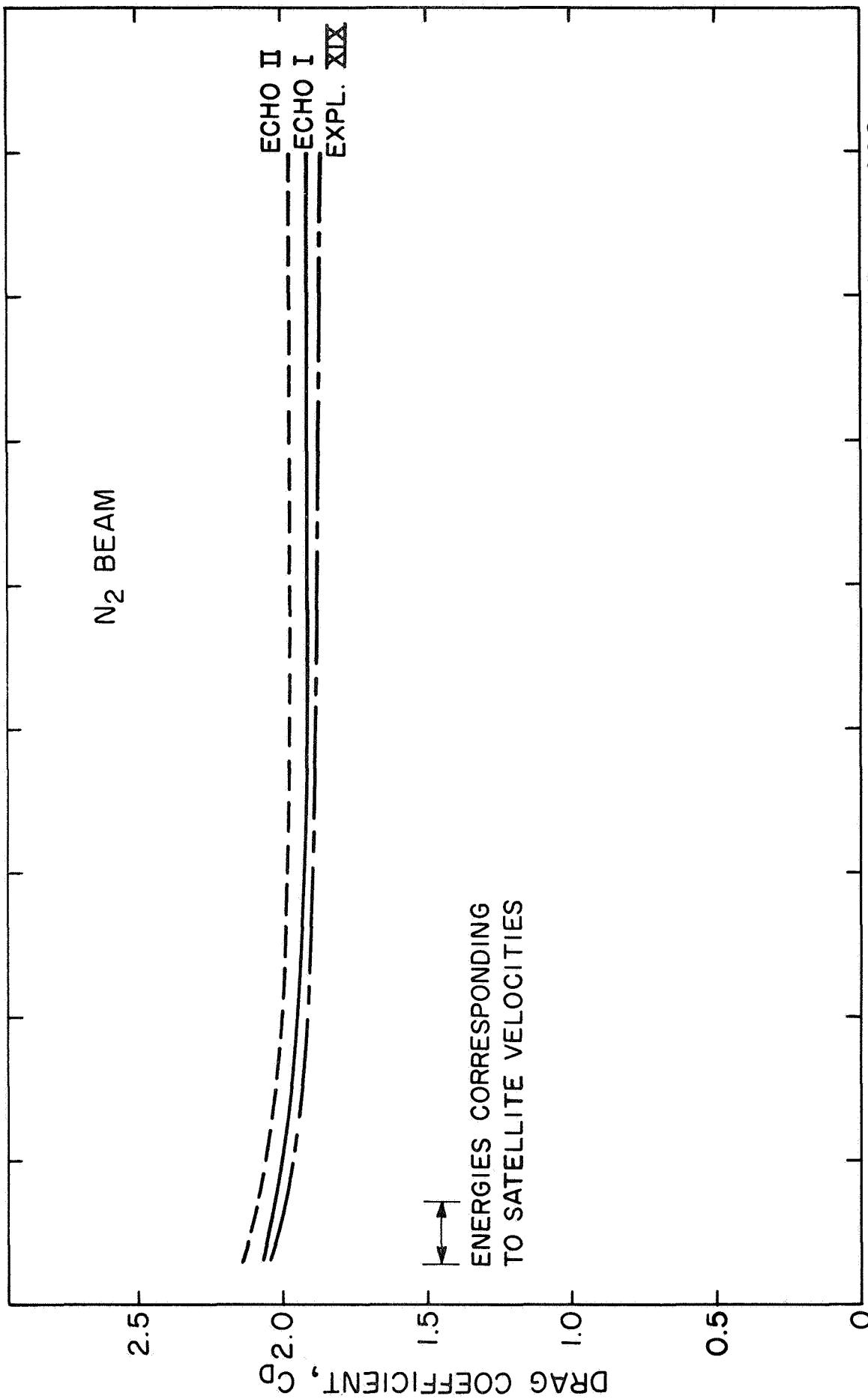


Figure 12. Average Drag Coefficients

the surface had rather sharp irregularities one might expect values closer to the Exho II curve. A typical photomicrograph of one of the painted surfaces mentioned in the Introduction is shown in Figure 13, and comparison with those of Figure 3 shows the painted surfaces to be relatively smooth. This would lead one to estimate that the drag coefficients for the painted surfaces would be somewhere around the lowest of the curves of Figure 12, to within a few percent (the order of the uncertainties of the curves of Figure 12 and the differences between curves for different surfaces).

The drag coefficients for the surfaces studied are seen to be slightly greater than 2 at low energies, a result one would also get by assuming that the reflected molecules are thermally accommodated to the surface. It should be pointed out, then, that the $C_D \approx 2$ for spheres obtained from the present experimental results come about because the appreciable positive value of $\frac{P_m}{P_o}$ for small angles is to a large extent cancelled by the negative values at larger angles. A body of a different shape might therefore give values of $C_D$ which are significantly different from 2.

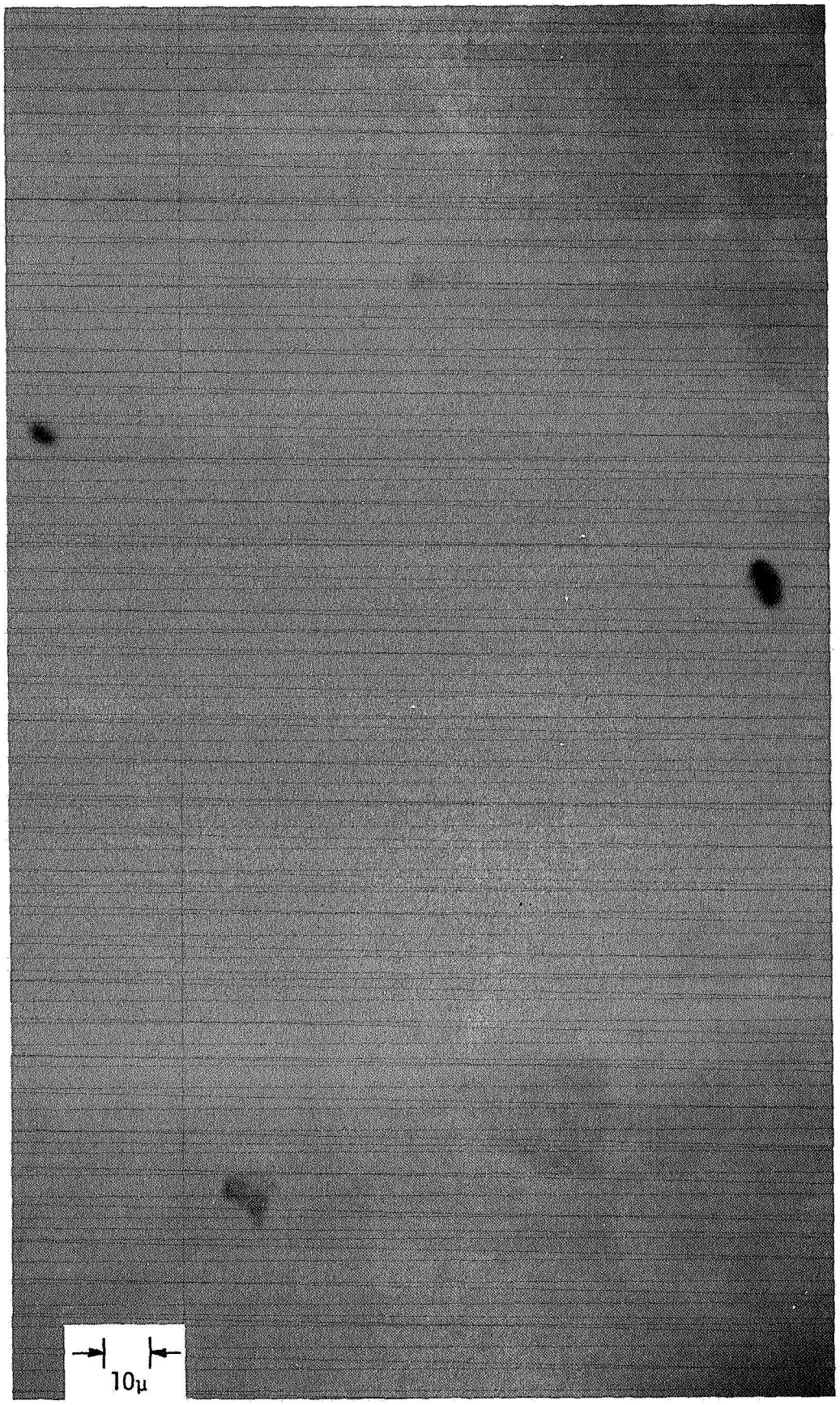


Explorer XXIV
(Avg. Paint = 3.06)

Figure 13. Photomicrograph of Painted Surface

## REFERENCES


1. Boring, J. W., "The Experimental Determination of Aerodynamic Drag on Solid Surfaces Simulating Satellite Motion," Proposal AST-NASA-38-62V, Research Laboratories for the Engineering Sciences, University of Virginia, Sept. 1962.

2. Boring, J. W. "A System for Investigating Molecule-Surface Interactions at Satellite Velocities," Report EP-4018-128-65U, Research Laboratories for the Engineering Sciences, University of Virginia, Nov. 1965.

3. Boring, J. W., "Momentum Transfer to Solid Surfaces by $N_2$ Molecules at Satellite Velocities," Report EP-4018-139-67U, Research Laboratories for the Engineering Sciences, University of Virginia, Feb. 1967.

4. Boring, J. W. "A Study of Systems for Producing High-Energy Monatomic Oxygen Beams," Report EP-4018-138-66U, Research Laboratories for the Engineering Sciences, University of Virginia, Sept. 1966.

5. Utterback, N. G. and Miller, G. H., Rev. Sci. Instr. 32, 1101 (1961).

6. Ignatenko and Myasnikov, A. S., Radiotekhnika i Elektronika 6, 2084 (1961). Translation: Foreign Technology Division, Wright-Patterson Air Force Base, FTD-TT-317, AD-288-987.

7. McDaniel, E. W., "Collision Phenomena in Ionized Gases," (John Wiley and Sons, New York, 1964).

8. Pearson, S and Wadsworth, N.J., J. Sci. Instr. 42, 150 (1965).

9. Jones, R. V., J. Sci. Instr. 38, 37 (1961).

10. Kaminsky, M., "Atomic and Ionic Impact Phenomena on Metal Surfaces," (Academic Press, New York, 1965).

NASA CR-66785

DISTRIBUTION LIST

| NAS1-2538 | Copies |
|---|---|
| NASA Langley Research Center<br>Langley Station<br>Hampton, Virginia 23365 | |
| Attention: Research Program Records Unit, Mail Stop 122 | 1 |
| Raymond L. Zavasky, Mail Stop 117 | 1 |
| John P. Mugler, Mail Stop 231 | 5 |
| NASA Ames Research Center<br>Moffett Field, California 94035 | |
| Attention: Library, Stop 202-3 | 1 |
| NASA Flight Research Center<br>P. O. Box 273<br>Edwards, California 93523 | |
| Attention: Library | 1 |
| Jet Propulsion Laboratory<br>4800 Oak Grove Drive<br>Pasadena, California 91103 | |
| Attention: Library, Mail 111-113 | 1 |
| NASA Manned Spacecraft Center<br>2101 Webster Seabrook Road<br>Houston, Texas 77058 | |
| Attention: Library, Code BM6 | 1 |
| NASA Marshall Space Flight Center<br>Huntsville, Alabama 35812 | |
| Attention: Library | 1 |
| NASA Wallops Station<br>Wallops Island, Virginia 23337 | |
| Attention: Library | 1 |
| NASA Electronics Research Center<br>575 Technology Square<br>Cambridge, Massachusetts 02139 | |
| Attention: Library | 1 |
| NASA Lewis Research Center<br>21000 Brookpark Road<br>Cleveland, Ohio 44135 | |
| Attention: Library, Mail Stop 60-3 | 1 |
| NASA Goddard Space Flight Center<br>Greenbelt, Maryland 20771 | |
| Attention: Library | 1 |

NASA CR-66785

DISTRIBUTION LIST

| NAS1-2538 | Copies |
|---|---|
| NASA John F. Kennedy Space Center<br>Kennedy Space Center, Florida 32899<br>Attention: Library, Code IS-CAS-42B | 1 |
| National Aeronautics and Space Administration<br>Washington, D. C. 20546 | |
| Attention: Library, Code USS-10 | 1 |
| Alfred Gessow, Code RR | 1 |
| Conrad P. Mook, Code RV-1 | 1 |
| NASA Scientific and Technical Information Facility<br>P. O. Box 33<br>College Park, Maryland 20740 | 10 plus reproducible |